ORGANOMETALLICS

pubs.acs.org/Organometallics Article

Statistical Analysis of Catalytic Performance in Ethylene/Methyl Acrylate Copolymerization Using Palladium/Phosphine-Sulfonate Catalysts

Shumpei Akita, Jing-Yao Guo, Falk W. Seidel, Matthew S. Sigman,* and Kyoko Nozaki*

Cite This: *Organometallics* 2022, 41, 3185−3196 Read Online

ACCESS | Metrics & More | Article Recommendations | Supporting Information

ABSTRACT: For various types of palladium complexes bearing phosphine-sulfonate (PS) ligands used in the coordination−insertion copolymerization of olefins with polar monomers, characteristic features of the ligands, such as electronic and steric properties, have been discussed to describe their catalytic performance. Aiming at further analysis of the literature data, here we report the development of a statistical method for how the ligand impacts the performance of a Pd-catalyzed copolymerization of ethylene and methyl acrylate (MA). During our investigation, ligand features important for the resultant molecular weight of the obtained polymers were identified. Consistent with previously suggested important parameters, the electron density on the palladium center and maximum width of the substituents on the phosphorus atom (B5) were found to be significant for catalyst performance. We also found that additional features impact reaction outputs. As an example, the lower occupancy of the palladium d_{z^2} orbital results in an increase of molecular weight and catalyst activity in both ethylene homopolymerization and ethylene/methyl acrylate copolymerization. Furthermore, it was predicted that a larger bite angle of the ligand increased the activity of ethylene/methyl acrylate copolymerization without impacting the molecular weight. On the basis of these machine learning predictions, three thiophene derived PS-type catalysts were synthesized and tested for MA/ethylene copolymerization. Unexpectedly, rather than the one predicted to enhance catalytic performance, a synthetic intermediate to this ligand exhibited higher activity albeit with the expense of molecular weight and MA incorporation. The inconsistency between the prediction and the experimental result is likely a result of insufficient training data for the catalyst with a different linker moiety. However, the unexpected finding that chlorination of the ligand backbone increases the overall catalyst performance will inspire an avenue for PS catalyst development.

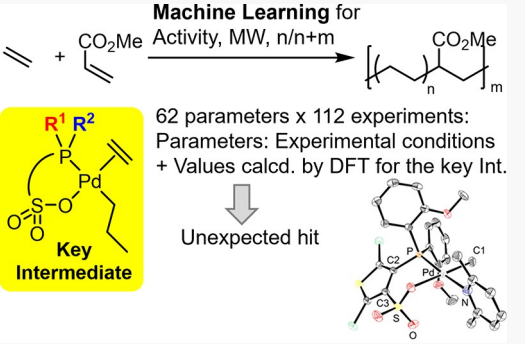

INTRODUCTION

Since the publication of the seminal work by Drent et al. in 2002,[1] extensive efforts have been devoted to the development of unsymmetrical bidentate ligands effective in promoting the palladium-catalyzed copolymerization of olefins with polar vinyl monomers.[2] Among the potent ligand types, phosphine-sulfonates (PS), which selectively facilitate the production of linear copolymers in high molecular weight (MW), have been the most investigated.[3] Various strategies have been developed over the years for the optimization of their catalytic performance, such as activity, product MW, and increased incorporation of polar monomers, and the impact of ligand characteristics has been scrutinized with considerable effort. Notably, Wucher et al. reported the ligand electronic effect in the copolymerization of ethylene with methyl acrylate (MA) promoted by di-*o*-anisylphosphino-benzenesulfonates (4-*R*-2-MeO-C_6H_3)$_2$P-C_6H_4-SO_3), where the presence of a strong electron donor on the phosphine component was observed to produce copolymers with increased MW, but with a concomitant decrease in catalytic activity (Scheme 1a).[4] In 2014, Nozaki and co-workers examined the steric impact of the phosphine substituents with the feature Sterimol B5, which describes the maximum width of the substituent.[3a,5] In both the homopolymerization of ethylene and its copolymerization with a variety of polar monomers, the B5 measure is positively correlated with the resultant MW (Scheme 1b). This association was postulated to be caused by the ability of bulky substituents to effectively shield the apical position of the metal center. To further evaluate the interplay of ligand electronic and steric features in their catalytic properties, we envisaged applying more sophisticated data science tools to comprehensively investigate the stereoelectronic factors that control the performance of this catalyst class.

Special Issue: Organometallic Chemistry Inspired by Maurice Brookhart

Received: February 3, 2022
Published: March 29, 2022

Scheme 1. Copolymerization of Ethylene and Methyl Acrylate with Palladium Phosphine-Sulfonate Catalysts

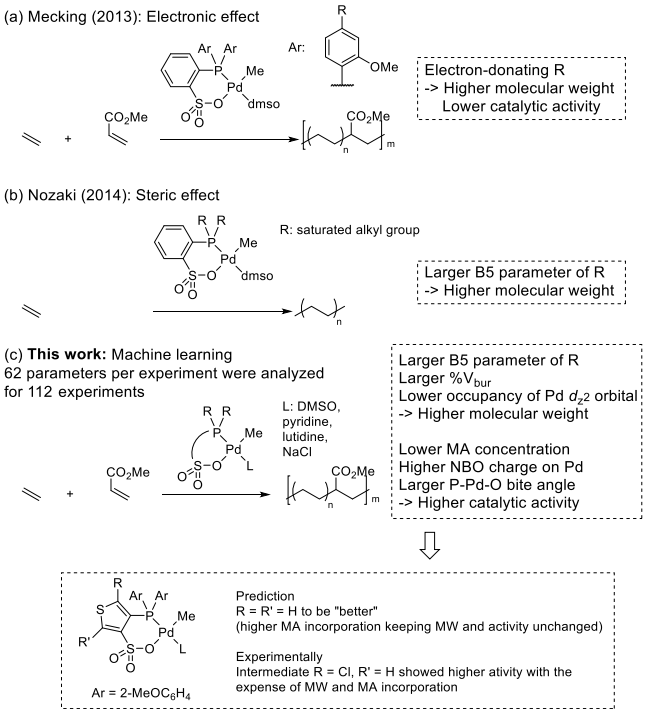

The product MW of a polymerization process is determined by the difference between the energies of activation ($\Delta\Delta G^{\ddagger}$) of chain propagation and chain transfer. Unfortunately, computational transition state studies with modern theoretical approaches (e.g., DFT calculations) are not adequate for the assessment of energy differences on this scale. For example, a difference of 1.0 kcal/mol, which is approximately the limit of accuracy in a DFT calculation for transition-metal catalysis, corresponds to an increase in MW by ∼4-fold.[6,7] Alternatively, the utilization of various molecular featurization tools, combined with machine learning algorithms, has been proven effective in the prediction of enantiomeric excess, a similarly sensitive reaction output.[8] For instance, in 2019, Denmark and co-workers demonstrated their process through the successful description of catalyst structural effects on the enantioselective thiol addition to *N*-acylimines, promoted by BINOL-derived phosphoric acids.[8a] In this study, the development of a steric descriptor that represents the entire conformer ensemble was the key to their success. In the same year, Sigman and co-workers reported the statistical modeling of data-mined literature results from a range of nucleophilic addition reactions to imines using DFT-derived physical organic parameters and the ability of the resulting model to provide out-of-sample predictions.[8b] We became interested in applying these types of data science methods to interrogate the performance of the Pd/PS system in ethylene polymerization and ethylene/MA copolymerization. Herein, we report the implementation of these types of workflows to explore which key catalyst features impact various polymerization metrics. Moreover, based on the statistical models constructed, we designed, synthesized, and tested three new thiophene derived PS-type catalysts. In contrast to our prediction, the designed thiophene-linker PS catalyst exhibited only modest activity while a synthetic intermediate in route to this catalyst provides some of the best catalyst performance metrics reported to date.

RESULTS AND DISCUSSION

Strategy. To initiate the investigation, we considered the general reaction mechanisms for chain propagation and chain transfer as suggested by previous studies (Scheme 2). DFT calculations suggested that chain propagation proceeds via ethylene coordination to an alkylpalladium intermediate (**1** → **2**), followed by cis/trans isomerization (**2** → **3**) and ethylene insertion (**3** → **4**), with the final one (**3** → **4**) being the rate-determining step of the desired polymerization reaction.[9] The rate-determining step for the chain transfer, which limits the polymer chain length, is ethylene dissociation from intermediate **3** to give **5** via β-hydride elimination. This mechanism suggests that intermediate **3** is the key intermediate located at the branching point to control the molecular weight of a polymer. Accordingly, we selected this general structure to build the requisite *in silico* feature set for statistical modeling applications.[10] The set of structures assessed in this study is tabulated in Figure 1.[3,9,11]

Comparative molecular field analysis (CoMFA)[11] was first employed to provide a spatial visualization of the catalyst

Scheme 2. Mechanism of Ethylene Polymerization Promoted by Palladium/Phosphine-Sulfonate Catalysts[a]

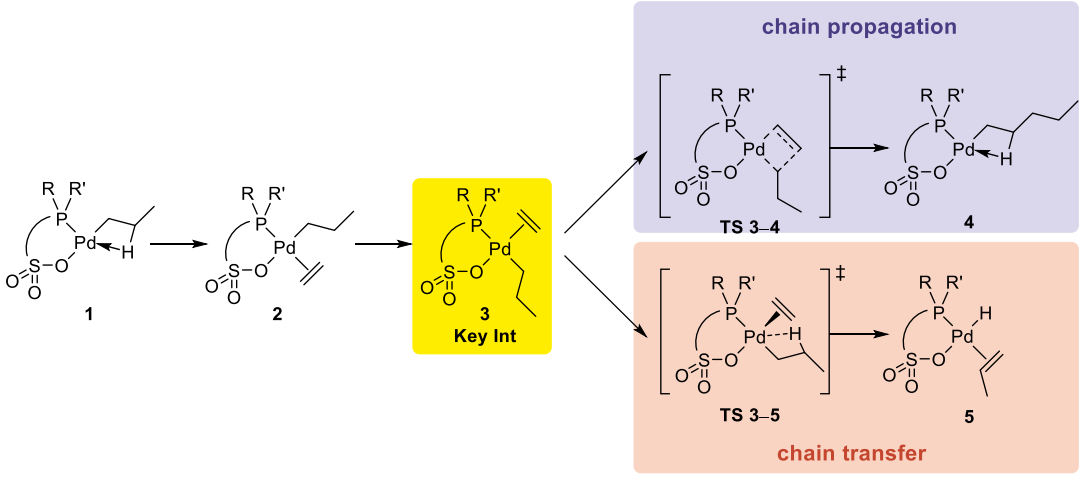

[a]Intermediate **3** is located at the branching point for chain propagation and chain transfer.

https://doi.org/10.1021/acs.organomet.2c00066
Organometallics 2022, 41, 3185−3196

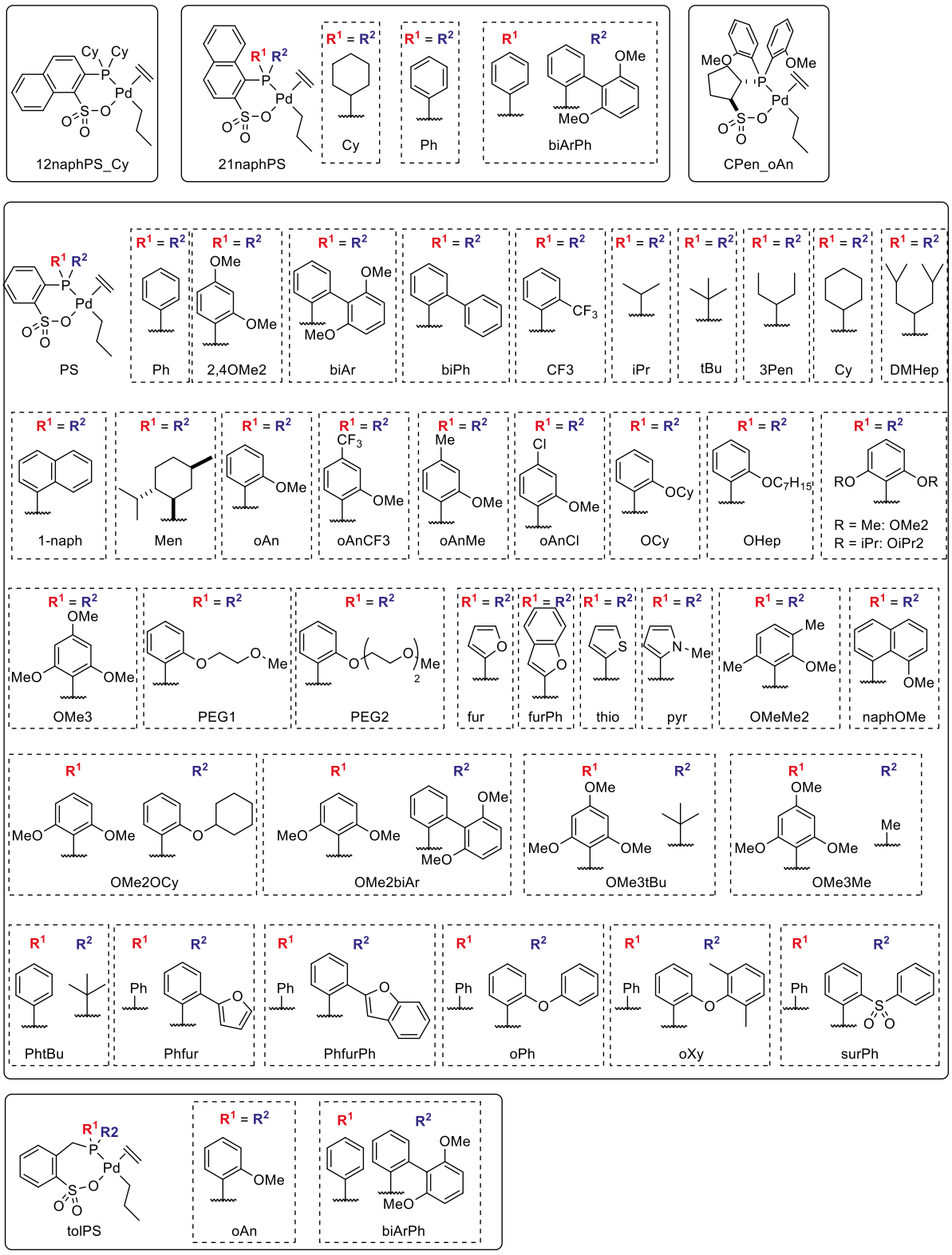

Figure 1. Structures of complexes used in the statistical analysis of polymerizations.

properties and their effect on the MW in ethylene homopolymerization. Subsequently, a statistical modeling study was carried out to determine how catalyst features impact (co)polymer properties (MW, polymerization activity, incorporation of polar monomer in case of E/MA copolymerization) in both the homopolymerization of ethylene (E) and the copolymerization of ethylene and methyl acrylate (MA).

In this paper, the polar monomer for copolymerization is limited to methyl acrylate because of bias in the reported data sets. In 120 entries, methyl acylate was used as polar monomer although there are 188 examples for copolymerization by Pd/

https://doi.org/10.1021/acs.organomet.2c00066
Organometallics 2022, 41, 3185−3196

PS. The original references for the data are listed in Tables S1 and S2 in the Supporting Information.

Data and Parameter Collection and Model Construction. Experimental data for ethylene polymerization promoted by methylpalladium complexes bearing PS ligands were collected from the literature. For analysis of both homopolymerization and copolymerization, the data used for model construction was filtered based on reaction temperature (80 °C for homopolymerization, 80−100 °C for E/MA copolymerization) and split randomly into training and test sets with a ratio of 80:20 (details in the Supporting Information). The same split was used for all analyses. Structures of intermediate **3** with a library of PS ligands (Figure 1) were calculated with the geometry optimization method B3LYP-D3(BJ)/[6-31G(d)+LANL2DZ], followed by a single point calculation with B3LYP-D3(BJ)/[6-311+G-(d,p)+SDD].

The CoMFA coordinates were set as described in Figure 2. The Pd atom was selected as the origin, and the square-planar

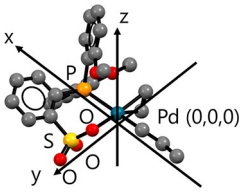

Figure 2. Definition of the coordinate grid.

coordination plane of Pd (i.e., the mean plane of Pd, the two ligating atoms in the PS ligand, and the bound carbon in the propyl group) was defined as the *xz* plane with the sulfonate group direction as the *y* positive. Although most of the ligands we employed are achiral, the complexes are chiral due to the conformation of the six-membered ring as depicted in Figure 3,

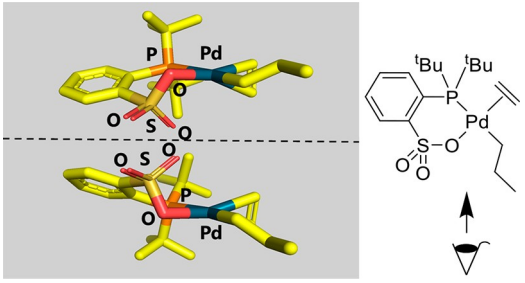

Figure 3. Example of mirror image parallel to coordination plane of palladium.

and as such, both mirror images with respect to the *xy* plane were equally considered in the analysis. The grid size was set to 1 Å. The information on grid occupation was converted to 10 orthogonal descriptors by principal component analysis (PCA). Conversion of grid occupancy to descriptors and compression by PCA was conducted in Open3dQSAR. Further analysis by linear regression was conducted on R ver. 3.6.1. The results were visualized on the grid with pseudocoefficients by using PyMOL ver. 2.2.3.

A wide variety of descriptors were collected for intermediate **3** from both the simulated complex structures and their corresponding ligand conformers (Figure 4), adding up to a total of 62 parameters (see the Supporting Information for

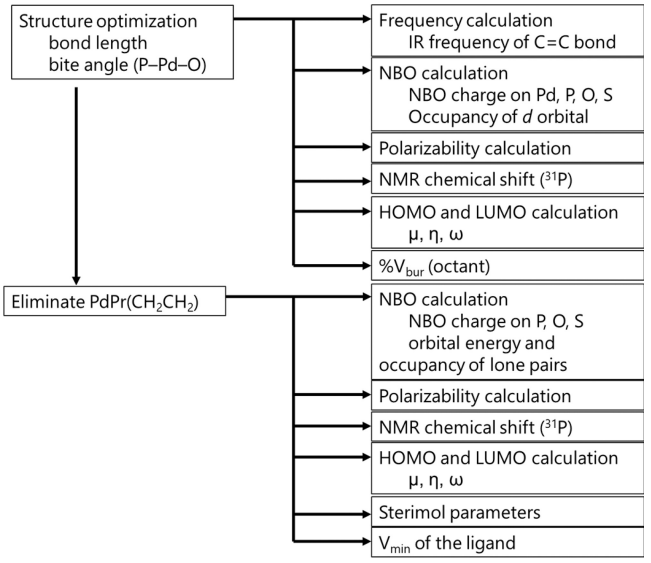

Figure 4. Procedure of parameter collection for machine learning.

details). A few notable examples are structural features (bond lengths, angles, percent buried volume ($\%V_{bur}$),[12] and Sterimol parameters), orbital information (HOMO and LUMO),[13] natural bond orbital (NBO) analysis of key atoms, the minima of electrostatic potential (V_{min}) localized around the ligating groups, polarizability, chemical shifts, and the stretching frequency for the ethylene bound to palladium.

The simulated molecular descriptors, along with reaction parameters (e.g., time, temperature, substrate concentration, catalyst loading), were utilized in the analysis of important reaction outputs. For ethylene homopolymerization, statistical models were developed for both molecular weight (MW, the M_n value) and activity, in the forms of log(MW) and log(activity), respectively. For ethylene/methyl acrylate copolymerization, incorporation efficiency (k) was added to the analyzed properties.[14] Incorporation efficiency represents how much the catalyst preferentially incorporates polar monomers during chain propagation, with the assumption that, without the bias introduced by the catalyst, incorporation of each monomer is in linear relation to its concentration. A large incorporation efficiency would allow for the direct synthesis of highly functionalized polyolefins with limited concentration of polar monomers during the preparation. The incorporation efficiency k was defined as

$$\begin{aligned}&(\text{incorporation ratio of MA [mol \%]})\\&\quad :(\text{incorporation ratio of ethylene [mol \%]})\\&= k\ (\text{incorporation efficiency})\cdot(\text{MA conc. [M]})\\&\quad :(\text{ethylene press. [MPa]})\end{aligned}$$

Thus

$$k\ (\text{incorporation efficiency}) = \frac{(\text{incorporation ratio of MA [mol \%]})\cdot(\text{ethylene press. [MPa]})}{(\text{incorporation ratio of ethylene [mol \%]})\cdot(\text{MA conc. [M]})} \quad (1)$$

For linear regression, preliminary models were regularized using Akaike's information criterion (AIC). In the random forest analysis, the number of predictors sampled for splitting at each node was tuned by using grid search. Subsequently, the

https://doi.org/10.1021/acs.organomet.2c00066
Organometallics 2022, 41, 3185−3196

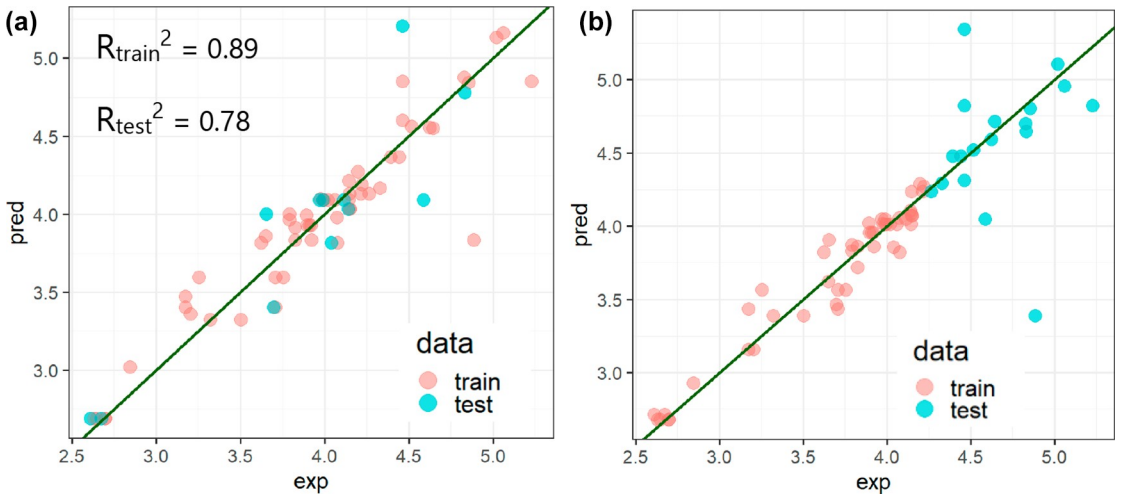

Figure 5. (a) Statistical analysis of molecular weight of ethylene polymerization with CoMFA using PLS. (b) Molecular weight prediction beyond the training set by CoMFA using linear regression.

Boruta function was used for elimination of nonexplaining descriptors. A 10-fold cross validation was chosen as a validation method. A number of algorithms (e.g., random forest analysis and support vector machine) were tested for their performances on this data set (details shown in the Supporting Information).

Comparative Molecular Field Analysis (CoMFA) for Molecular Weight (MW) Analysis. The result of the statistical analysis of log(MW) is shown in Figure 5a. Values of the coefficient of determination for training data sets, R_{train}^2, and of the coefficient of determination for test data sets, R_{test}^2, are 0.89 and 0.78, respectively, suggesting a reasonably robust model. The catalysts in the data set can be divided into two classes: the major class includes ligands that have the same two substituents on the phosphorus atom while the minor class (9 out of 71 entries) has two different substituents on the phosphorus atom wherein P atom is a stereogenic center. The model produced a significantly better prediction for the major class, and unsurprisingly, due to limited representation in the training set, the minor class is more poorly predicted.

Partial-least-squares (PLS) pseudocoefficient maps can be visualized on the grid. The visualized map on Pd/PS substituted by 2-[2′,6′-$(MeO)_2C_6H_3$]C_6H_4 is depicted in Figure 6. The red space is positively correlated with an increase in the polymer MW, whereas the blue space is the opposite. As marked by a black dashed circle in the bottom of Figure 6, the apical position ~3 Å from the palladium center is highlighted in red, meaning occupation of this position by a substituent is correlative with an increase in the MW of the polymer. The result is consistent with our previous hypothesis.[3a] Namely, the bulkiness of the substituent occupying the apical position is essential to obtaining higher MW, because it blocks the β-hydrogen from the palladium and thus suppresses the chain-terminating β-hydride elimination. As circled by the white dashed line in Figure 6, there is a blue area in the outside of ethylene coordinated to the palladium center. This area is occupied when the palladium−ethylene bond becomes long; thus this should correspond to the weak coordination of ethylene. When the coordination of ethylene is weak in intermediate **3**, the ethylene dissociation transition state (TS) (**3** → **5**) is accelerated reducing the MW of the polymer.

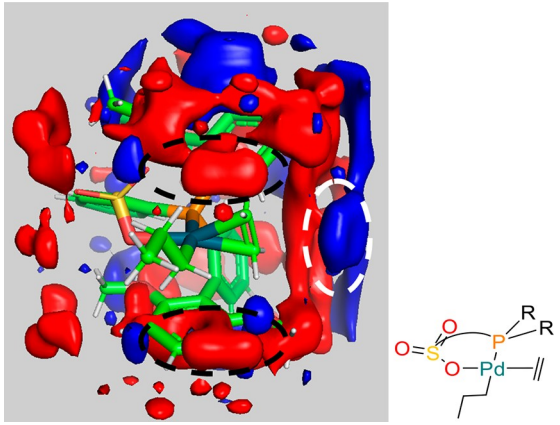

Figure 6. PLS pseudocoefficient map drawn on palladium/phosphine-sulfonate complex substituted by 2-[2′,6′-$(MeO)_2C_6H_3$]C_6H_4 (red, positive; blue, negative).

Aiming to confirm whether extrapolation was possible, data in the limited region was used as training data with the boundary set as log(MW) = 4.25. The result is shown in Figure 5b. The trend of the accuracies for each data was similar to the calculation with interpolation shown in Figure 5a, while the extrapolation analysis shown in Figure 5b contained a relatively larger error. Several data are significantly poorly predicted with examples for the Pd/PS catalyst in which the phosphorus atom is substituted by 2,4,6-$(OMe)_3C_6H_2$ and *t*Bu (the data (experimental, predicted) = (4.89, 3.83)).

As described above, CoMFA successfully produced a prediction model for the molecular weight of the obtained polymer using a Pd/PS system. It also suggested that 3D information on the catalysts' effect on the MW can be extracted. Next, to explore the effect of catalyst properties more deeply, we probed the system by using DFT-derived properties to build more interpretable statistical models.

Statistical Models for Ethylene Homopolymerization. Using the parameter library as shown in Figure 4, we first explored correlating the MW for the homopolymerization of ethylene. LASSO regression was first used to build a preliminary model (Figure 7a), with R_{train}^2 = 0.84 and R_{test}^2

https://doi.org/10.1021/acs.organomet.2c00066
Organometallics 2022, 41, 3185−3196

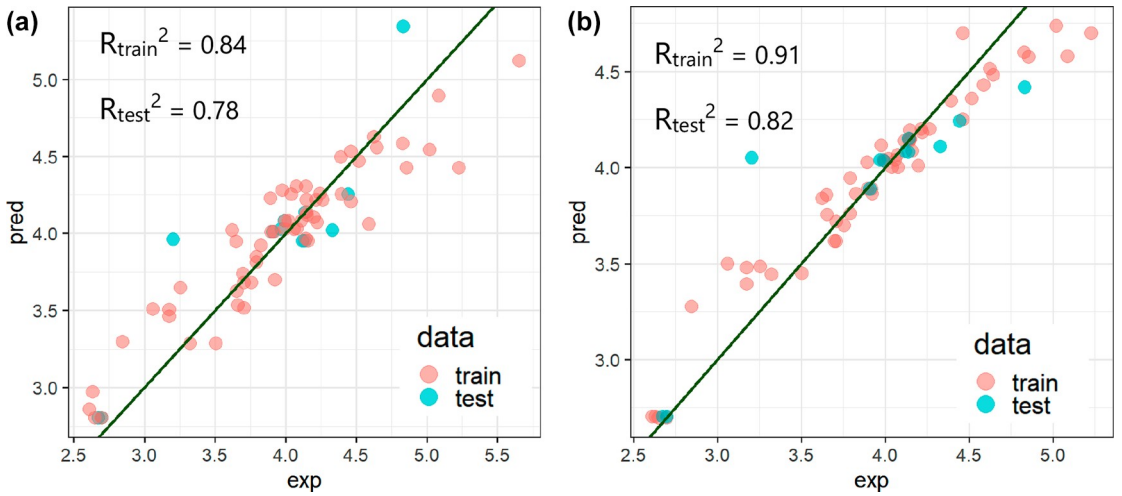

Figure 7. Statistical analysis of log(MW) of ethylene polymerization using (a) LASSO regression and (b) random forest.

= 0.78, suggesting a function/parameter combination of the model fits for training and test data.

Next, random forest (RF) was chosen for further statistical correlation of the ethylene homopolymerization data set. In this case, not only the MW of the resulting polymer but also the measured catalytic activity was examined. The calculated models were evaluated via R_{train}^2 and R_{test}^2 from the training and test sets, respectively. The resulting statistical analysis of the MW of the polymer and polymerization activity using random forest are shown in Figures 7b and 8, respectively.

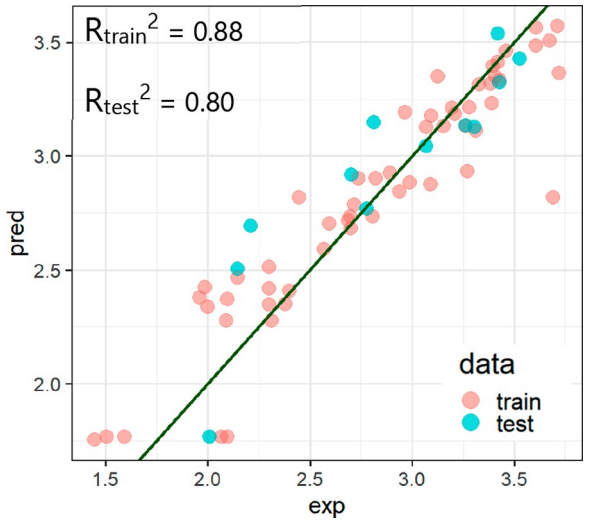

Figure 8. Statistical analysis of activity of ethylene polymerization using random forest.

R_{train}^2 and R_{test}^2 were calculated for each prediction. In both predictions, R_{train}^2 and R_{test}^2 are greater than 0.85 and 0.80 respectively, thus showing good agreement.

The important features impacting the RF fit for the MW analysis are depicted in Table 1 with the most heavily weighted parameter being the NBO charge on the palladium center. Similarly, the catalytic activity was analyzed. In this case, ^{31}P NMR chemical shifts were found to be the most important parameter (Table 2).

Ethylene/Methyl Acrylate Copolymerization. Encouraged by the meaningful analysis of the ethylene homopolymerization, we explored the ethylene/MA copolymerization. First, the MW of the obtained MA/ethylene copolymers was statistically analyzed by LASSO regression (Figure 9a). R_{train}^2 and R_{test}^2 were 0.65 and 0.24, respectively, suggesting a poor explanation of the MW in the case of MA/ethylene copolymerization. The random forest approach was further applied to E/MA copolymerization results by Pd/PS. The analyses of three features of the polymerization results, namely the MW of the copolymer, catalytic activities, and incorporation efficiency of MA into the polymer chain are depicted in Figure 9b–d. As shown in Figure 9b,d in the cases of MW and MA incorporation efficiency analysis, R_{train}^2 and R_{test}^2 are larger than 0.85 and 0.80, respectively. In contrast, in the case of polymerization activity (Figure 9c), R_{test}^2 is lower than 0.75, suggesting the model is insufficient although R_{train}^2 is larger than 0.85. In the incorporation efficiency analysis, R_{train}^2 and R_{test}^2 were 0.91 and 0.82, respectively. For the MW of the copolymer, R_{train}^2 and R_{test}^2 were calculated with randomly separated training/test data sets through 100 iterations. The averages of R_{train}^2 and R_{test}^2 were 0.92 ± 0.009 and 0.73 ± 0.1, suggesting the consistently high validation score supports the validity of the model (see Table S6 for details).

Table 1. Important Parameters for Prediction of MW of Ethylene Polymer

parameter	importance
NBO charge on Pd	1.61
average of B5 value[a]	1.21
^{31}P NMR chemical shift	1.21
occupancy of d_{z^2}	1.04
NBO charge on S	0.94

[a]Average of B5 value of the two substituents on phosphorus atom.

Table 2. Important Parameters for Prediction of Polymerization Activity of Ethylene Polymerization

parameter	importance
^{31}P NMR chemical shift	1.59
average of *L* value[a]	1.50
NBO charge on Pd	1.48
occupancy of d_{z^2}	0.98
reaction time	0.94

[a]Average of *L* value of the two substituents on phosphorus atom.

https://doi.org/10.1021/acs.organomet.2c00066
Organometallics 2022, 41, 3185−3196

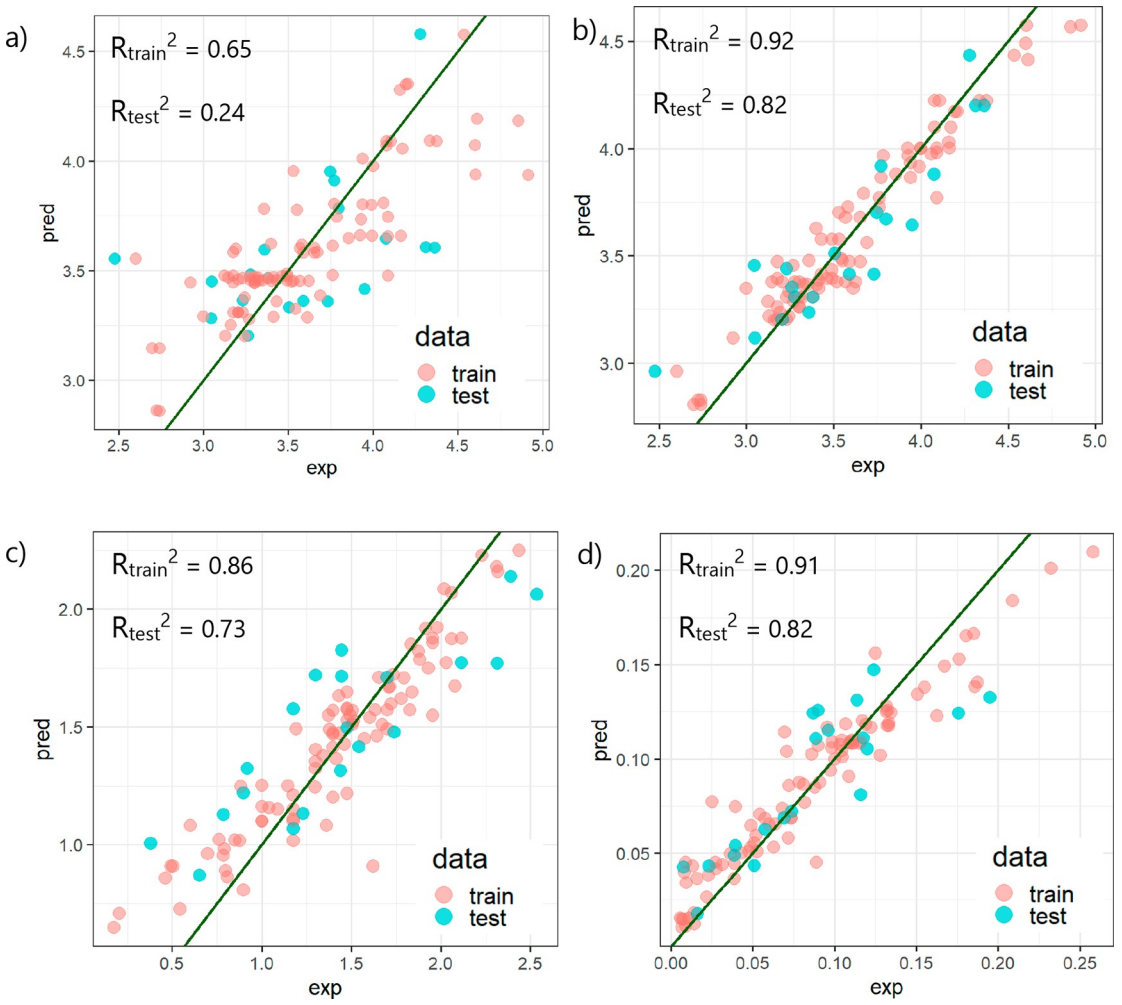

Figure 9. Statistical analysis of MW of E/MA copolymerization using (a) LASSO regression and (b) random forest and statistical analysis of (c) polymerization activity and (d) incorporation efficiency of E/MA copolymerization using random forest.

The important descriptors for the MW of the copolymer (Figure 9b) are summarized in Table 3. The two most important parameters are the average of the B5 parameter and $\%V_{bur}$. The important descriptors for the polymerization activity of E/MA copolymerization (Figure 9c) are shown in Table 4. Finally, the incorporation efficiency of MA into the copolymer (defined in eq 1, *vide supra*) was analyzed (Figure 9d), and the important descriptors are shown in Table 5.

Table 3. Important Parameters for Prediction of MW of Ethylene/Methyl Acrylate Copolymer

parameter	importance
average of B5 parameter	3.20
$\%V_{bur}$	2.02
occupancy of d_{z^2}	1.92
temperature	1.52
μ^a	1.16

[a]Absolute chemical potential.

Table 4. Important Parameters for Prediction of Polymerization Activity in E/MA Copolymerization

parameter	importance
MA concentration	2.82
NBO charge on Pd	1.84
bite angle	1.57
ethylene pressure	1.48
length of Pd−ethylene	1.41

Table 5. Important Parameters for Prediction of Incorporation Efficiency of MA in Ethylene/Methyl Acrylate Copolymer

parameter	importance
NBO charge on Pd	0.0308
energy level of lone pair of P	0.0211
MA concentration	0.0210
$\%V_{bur}$	0.0177
bite angle	0.0172

Prediction of Catalysts Candidates and Synthesis. On the basis of the above analysis, we designed new Pd/PS-type catalysts as follows. Many of the descriptors describe a trade-off between the molecular weight of the polymer and polymerization activity. Also, incorporation of MA decreases the activity. Among the descriptors we examined, we focused our attention on the P−Pd−O bite angle because its importance for polymerization activity was relatively significant but its impact on the polymer molecular weight was predicted to be modest. Accordingly, we assumed that an increase in bite

https://doi.org/10.1021/acs.organomet.2c00066
Organometallics 2022, 41, 3185−3196

Table 6. Predicted and Experimental Results for Palladium Complexes Ligated by Varying Ring Linker Phosphine-Sulfonate[a,b]

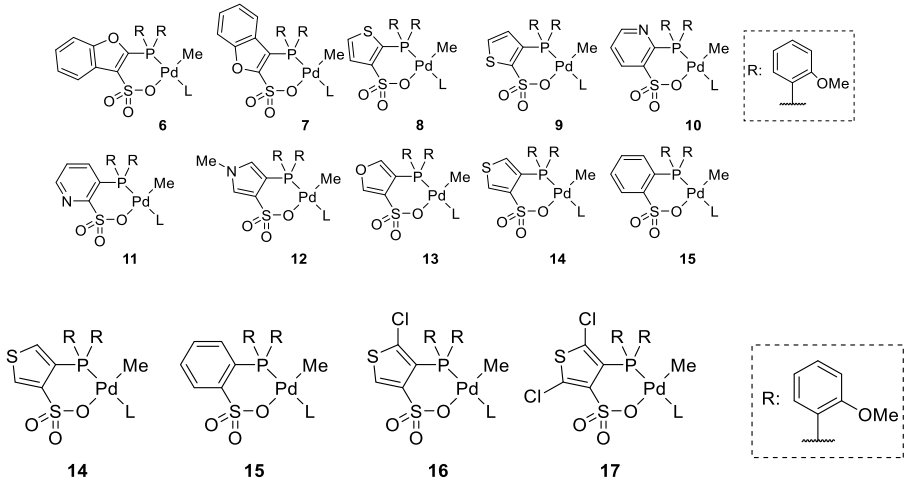

		predicted			experimental			
entry	cat.	M_n (10^3)	activity (g mmol^{-1} h^{-1})	IR[c] (mol %)	M_n (10^3)	PDI	activity (g mmol^{-1} h^{-1})	IR[c] (mol %)
1	**6**	6.1	20	2.5	–	–	–	–
2	**7**	10.3	17	2.1	–	–	–	–
3	**8**	14.8	54	3.6	–	–	–	–
4	**9**	14.0	59	2.0	–	–	–	–
5	**10**	17.4	30	3.9	–	–	–	–
6	**11**	17.4	44	3.8	–	–	–	–
7	**12**	11.1	76	4.5	–	–	–	–
8	**13**	17.6	79	4.3	–	–	–	–
9	**14**	17.6	91	4.4	1.9	2.0	64	3.4
10	**15**	19.0	117	3.4	12.1	2.2	152	5.0
11	**16**	17.6	41.9	2.6	2.5	2.1	339	2.7
12	**17**	17.4	40.3	2.6	6.6	2.1	156	3.8

[a]The prediction was done for the following conditions: catalyst (10 μmol), methyl acrylate (1.0 M in toluene, total 20 mL), and ethylene (3.0 MPa) in a 50 mL autoclave for 3 h at 80 °C. [b]The polymerizations were done under the following conditions: catalyst (0.25 μmol in 100 μL of CH_2Cl_2), methyl acrylate 3 mL, toluene 11.9 mL, and ethylene (3.0 MPa) in a 50 mL autoclave for 1.5 h at 80 °C. [c]The incorporation ratio (IR) for the prediction was calculated from the predicted incorporation efficiency, and the IR for experiments was determined by quantitative ^{13}C NMR analysis.

angle would result in higher polymerization activities without a decrease in polymer molecular weight. To increase the bite angle, phosphine-sulfonate complexes bearing five-membered ring linkers, **6**–**9** and **12**–**14**, were evaluated with our model, although it should be noted that this type of catalyst is not included in the training data. Therefore, we were aware that these new catalysts would be considered significant extrapolations of the statistical models. To investigate the effect of the heteroatom, complexes **10** and **11** were also considered. The calculated values are shown in Table 6 (*vide infra* for complexes **16** and **17**). As shown, complex **14** having a 3,4-thienylene linker was predicted to give a polymer molecular weight and polymerization activity comparable to those of the standard catalyst **15** (compare entries 9 and 10 in Table 6). In addition, the incorporation ratio of methyl acrylate with **14** is predicted to be higher than that with **15**. On the basis of this prediction, we next synthesized **14**.

Synthesis and Structural Analyses of 14 and Its Derivatives 16 and 17. To synthesize complex **14**, the following route toward ligand precursors **20**–**22** (Scheme 3a) was established: isobutyl ester **19** derived from sulfonyl chloride **18** was mixed with bis(*o*-anisyl) chlorophosphine and then treated at 0 °C with TMPMgCl·LiCl, furnishing the dichloro ligand precursor **20**. Double dehalogenation of **20** using catalytic Pd/C with an excess of magnesium metal in MeOH gave the desired dihydro ligand precursor **21** in 64% isolated yield. Monochloro ligand precursor **22** was also accessed in 93% yield by the selective and quantitative C–Cl magnesiation of the 2-position but not the 5-position of **20**. While the dihydro ligand derivative **21** readily oxidized in air, the electron-deficient chlorinated derivatives **20** and **22** were more oxygen tolerant, which allowed their purification by standard benchtop column chromatography. Ligands **20**–**22** were first allowed to react with PdMeCl(cod) furnishing intermediate phosphine–sulfonic ester complexes, which upon addition of 2,6-lutidine quantitatively interconverted to the respective palladium complexes **14**, **16**, and **17** (Scheme 3b). After crystallization from the crude mixtures, **14**, **16**, and **17** could be isolated as colorless crystals in 76, 88, and 94% yield, respectively.

The molecular structures of complexes **14**, **16**, and **17** were further analyzed by single crystal X-ray diffraction (Figure 10). Larger P–Pd–O angles were detected in complex **14** (97.08(4)°) as well as monochlorinated **16** (96.30(3)°) when compared to the conventional phenylene linker P/S catalyst **15** (95.00(6)°; CCDC-659797). In contrast, the dichlorinated **17** (86.91(5)°) exhibited a much smaller bite angle. A possible explanation is that, in **17**, the larger chlorine

https://doi.org/10.1021/acs.organomet.2c00066
Organometallics 2022, 41, 3185–3196

Scheme 3. Syntheses of (a) Ligands 20−22 and (b) Complexes 14, 16, and 17

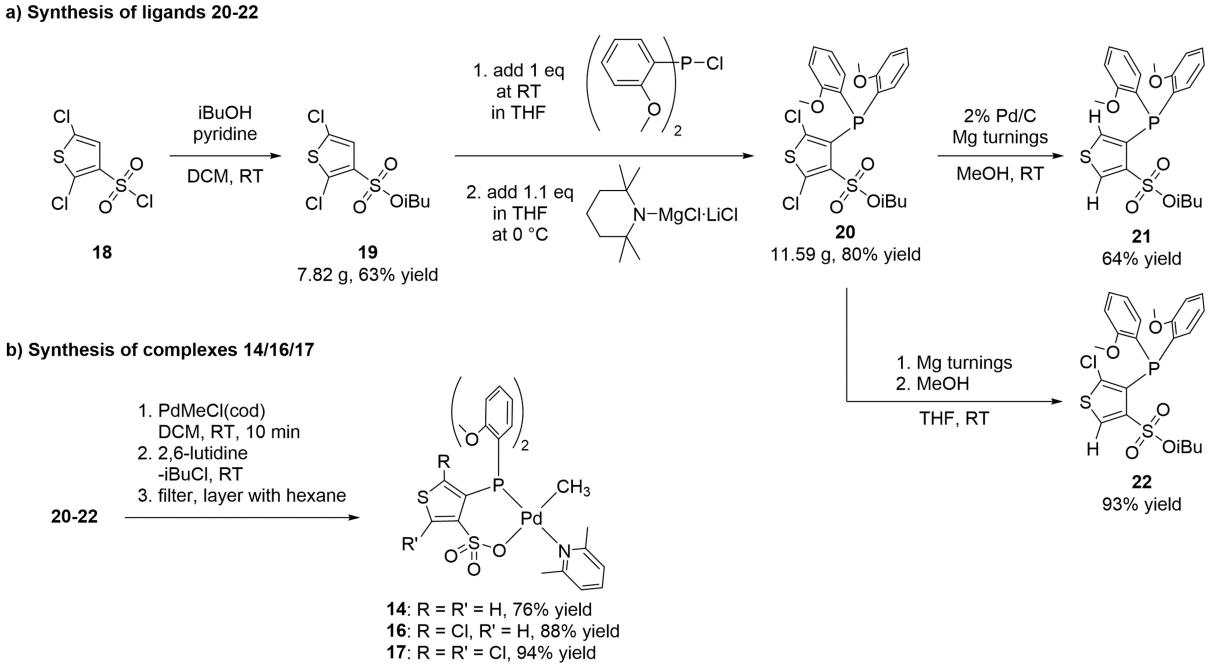

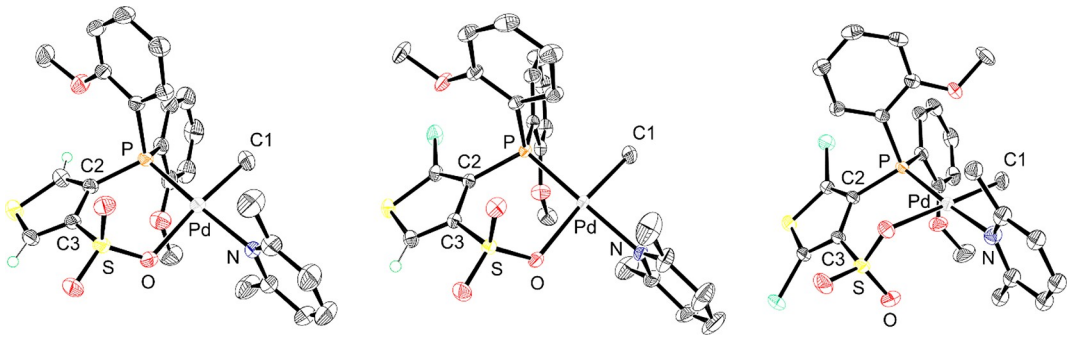

Figure 10. Molecular structures of **14** (left), **16** (middle), and **17** (right) in the crystal. (ORTEP drawn at 50% probability; all but the thiophene H atoms and the cocrystallized CH_2Cl_2 molecule in **16** are omitted for clarity; only one disorder position for the 2,6-lutidine ligands in **14**, **16** and **17** and a methoxy group in **17** are shown; data for the second disorder position are shown in brackets respectively.) Selected bond lengths (Å) and angles (deg) for **14**: Pd−C1 2.026(3), Pd−P 2.2287(5), Pd−O 2.1626(17), Pd−N 2.12(2) (2.131(3)), C1−Pd−P 87.94(6), C1−Pd−N 91.4(9) (89.29(14)), P−Pd−O 97.08(4), O−Pd−N 83.7(9) (85.64(14), O−S−C3−C2 54.39(11); sum of angles around Pd (C1/P/O/N): 360.12 (359.95). For **16**: Pd−C1 2.0378(16), Pd−P 2.2468(4), Pd−O 2.1809(10), Pd−N 2.15(3) (2.136(3)), C1−Pd−P 88.66(5), C1−Pd−N 89.5(10) (89.41(11), P−Pd−O 96.30(3), O−Pd−N 85.6(10) (85.62(10)), O−S−C3−C2 57.46(12); sum of angles around Pd (C1/P/O/N): 360.06 (359.99). For **17**: Pd−C1 2.028(2), Pd−P 2.2309(6), Pd−O 2.1728(13), Pd−N 2.127(8) (2.121(6)), C1−Pd−P 93.21(8), C1−Pd−N 87.3(2) (87.23(18)), P−Pd−O 86.91(5), O−Pd−N 92.47(19) (92.57(17)), O−S−C3−C2 22.33(19); sum of angles around Pd (C1/P/O/N): 359.89 (359.92).

substituent on the 2-position of the thiophene ring causes a rotational restriction of the sulfonate group, whereas for **14** and **16** a smaller hydrogen substituent on the analogous positions allows a rotation and relaxation of the same. The restriction is also reflected in the O−S−C3−C2 angles for **14** (54.39(11)°) and **16** (57.46(12)°), which lead to a significantly larger tilt of the Pd-coordinated sulfonate oxygen out of coplanarity with the thiophene unit in comparison with **17** (22.33(19)°). Still, all three catalysts show near-perfect square-planar coordination environments with sums of angles around the Pd atoms between 359.89 and 360.12° for **14**, **16**, and **17**.

Experimental Evaluation of Thiophene-Based Catalysts 14, 16, and 17 and Comparison with Predictions. We then applied the new catalysts **14**, **16**, and **17** to the copolymerization of methyl acrylate with ethylene and compared their performances with that of the reference catalyst **15** under the same reaction conditions. The results are summarized in Table 6. The reference catalyst **15** exhibited lower M_n, higher activity (entry 4), and higher incorporation ratio under our experimental conditions (12.1 kg mol^{-1}, 152 kg mol^{-1} h^{-1}, 5.0 mol %), compared to the predicted values in Table 6, entry 10 (5.2 kg mol^{-1}, 123 kg mol^{-1} h^{-1}, 4.2 mol %). The difference may be attributed to the lower catalyst loading (0.25 μmol) compared to the value used for prediction (10 μmol).

Contrary to our expectations in Table 6 (similar M_n and activity with slightly higher incorporation ratio with **14** compared to **15**), the dihydro complex **14** produced an ethylene/MA copolymer with a much lower M_n of 1.9 kg

https://doi.org/10.1021/acs.organomet.2c00066
Organometallics 2022, 41, 3185−3196

mol^{-1} and catalytic activity of 64 g $mmol^{-1}$ h^{-1} with a lower incorporation ratio of 3.4% (Table 6, entry 9). Of particular note and rather unexpectedly, 5-monochlorinated **16** showed an M_n of 2.7 kg mol^{-1} with a more than 2-fold increase in activity of 339 kg mol^{-1} h^{-1} albeit with a lower MA incorporation of 2.7% (Table 6, compare entries 9 and 10). The 2,5-dichlorinated catalyst **17** further increased the M_n to 3.8 kg mol^{-1} with 156 kg mol^{-1} h^{-1} activity and 3.4% incorporation of MA (Table 6, entry 12). We then calculated the prediction values for **16** and **17** with our model. The results are shown as entries 11 and 12 in Table 6. The activities for **16** and **17** were both predicted to be lower than that for **14** or **15**, which is inconsistent with the higher activity experimentally determined using **16**.

Thus, the relationship of the molecular structures from single crystal X-ray crystallography to the catalytic performance as of now is not clear. However, the unexpected observation that increased chlorination of the thiophene linker led to increased catalyst performances for **16** and **17** over **14** suggests why the predictions from the statistical models do not match the observed results. Specifically, the training set mainly contained catalysts with ligand backbones containing six-membered phenyl linkers, and P/S catalyst examples containing five-membered ligand backbones remain rare in the literature. Furthermore, the electronic perturbation due to the linker is also not represented in the literature. Therefore, the poor prediction of the experimental performances of the thiophene derived catalysts **14**, **16**, and **17** is perhaps not surprising. Nevertheless, the performances of the novel chlorinated thiophene sulfonate catalysts **16** and **17** comparable with that of the well-established reference system **15** were unexpected and provide a foundation for exploring novel PS-type catalysts in the future.

CONCLUSION

Molecular features impacting the ethylene homopolymerization and copolymerization with MA catalyzed by palladium complexes ligated by phosphine-sulfonate were analyzed by means of a number of data science tools. These analyses led to the identification of ligand features important for the resultant molecular weights of the obtained polymers: (1) The larger maximum width of the substituents on the phosphorus atom described by the B5 parameter results in higher molecular weight in both ethylene homopolymerization and ethylene/methyl acrylate copolymerization. (2) The higher electron density on the palladium center causes higher molecular weight by sacrificing catalyst activity in both types of polymerization reactions. While these findings are consistent with the reported tendencies, some new findings were uncovered. (3) The lower occupancy of the palladium d_{z^2} orbital results in increases of molecular weight and catalyst activity in both types of polymerization reactions. (4) The larger bite angle of the ligand increased the activity of the ethylene/methyl acrylate copolymerization without affecting the molecular weight. On the basis of these predictions, three Pd/(partially chlorinated) thiophene based PS complexes were synthesized. Unexpectedly, the chlorinated complexes led to higher catalytic activity in the MA/ethylene copolymerization. One explanation for the experimental deviations from the statistical models likely lies in the underrepresentation of five-membered ring type PS catalysts and halogenated linkers in model training. Lengths/widths of ligands or bite angles are not solely steric factors, but these are hybrid parameters that likely account for the electronic impact as well. Future work will exploit this new finding in the development of improved catalysts while also incorporating data to enhance the predictive statistical models.

ASSOCIATED CONTENT

Supporting Information

The Supporting Information is available free of charge at https://pubs.acs.org/doi/10.1021/acs.organomet.2c00066.

Details of the calculations and experiments (PDF)

Accession Codes

CCDC 2109317−2109318 and 2109322 contain the supplementary crystallographic data for this paper. These data can be obtained free of charge via www.ccdc.cam.ac.uk/data_request/cif, or by emailing data_request@ccdc.cam.ac.uk, or by contacting The Cambridge Crystallographic Data Centre, 12 Union Road, Cambridge CB2 1EZ, U.K.; fax: +44 1223 336033.

AUTHOR INFORMATION

Corresponding Authors

Kyoko Nozaki − *Department of Chemistry and Biotechnology, Graduate School of Engineering, The University of Tokyo, Bunkyo-ku, Tokyo 113-8656, Japan*; orcid.org/0000-0002-0321-5299; Email: nozaki@chembio.t.u-tokyo.ac.jp

Matthew S. Sigman − *Department of Chemistry, College of Science, The University of Utah, Salt Lake City, Utah 84112, United States*; Email: matt.sigman@utah.edu

Authors

Shumpei Akita − *Department of Chemistry and Biotechnology, Graduate School of Engineering, The University of Tokyo, Bunkyo-ku, Tokyo 113-8656, Japan*

Jing-Yao Guo − *Department of Chemistry, College of Science, The University of Utah, Salt Lake City, Utah 84112, United States*

Falk W. Seidel − *Department of Chemistry and Biotechnology, Graduate School of Engineering, The University of Tokyo, Bunkyo-ku, Tokyo 113-8656, Japan*

Complete contact information is available at: https://pubs.acs.org/10.1021/acs.organomet.2c00066

Notes

The authors declare no competing financial interest.

ACKNOWLEDGMENTS

A part of this work was supported by JSPS KAKENHI JP18H05259 and JST ERATO JPMJER2103. The theoretical calculations were performed using computational resources provided by the Research Center for Computational Science, National Institutes of Natural Sciences, Okazaki, Japan. S.A. thanks the Program for Leading Graduate Schools (MERIT) from the JSPS. M.S.S. thanks the National Science Foundation (CHE-1763436) for funding.

REFERENCES

(1) Drent, E.; van Dijk, R.; van Ginkel, R.; van Oort, B.; Pugh, R. I. Palladium catalysed copolymerisation of ethene with alkylacrylates: polar comonomer built into the linear polymer chain. *Chem. Commun.* **2002**, 744−745.

(2) For reviews, see: (a) Nakamura, A.; Ito, S.; Nozaki, K. Coordination-Insertion Copolymerization of Fundamental Polar Monomers. *Chem. Rev.* **2009**, *109*, 5215−5244. (b) Ito, S.; Nozaki,

K. Coordination-Insertion Copolymerization of Polar Vinyl Monomers by Palladium Catalysts. *Chem. Rec.* **2010**, *10*, 315−325. (c) Nakamura, A.; Anselment, T. M. J.; Claverie, J.; Goodall, B.; Jordan, R. F.; Mecking, S.; Rieger, B.; Sen, A.; van Leeuwen, P. W. N. M.; Nozaki, K. Ortho-Phosphinobenzenesulfonate: A Superb Ligand for Palladium-Catalyzed Coordination-Insertion Copolymerization of Polar Vinyl Monomers. *Acc. Chem. Res.* **2013**, *46*, 1438−1449. (d) Carrow, B. P.; Nozaki, K. Transition-Metal-Catalyzed Functional Polyolefin Synthesis: Effecting Control through Chelating Ancillary Ligand Design and Mechanistic Insights. *Macromolecules* **2014**, *47*, 2541−2555. (e) Baier, M. C.; Zuideveld, M. A.; Mecking, S. Post-Metallocenes in the Industrial Production of Polyolefins. *Angew. Chem., Int. Ed.* **2014**, *53*, 9722−9744. (f) Ito, S. Chain-Growth Polymerization Enabling Formation/Introduction of Arylene Groups into Polymer Main Chains. *Polym. J.* **2016**, *48*, 667−677. (g) Ito, S. Palladium-Catalyzed Homo- and Copolymerization of Polar Monomers: Synthesis of Aliphatic and Aromatic Polymers. *Bull. Chem. Soc. Jpn.* **2018**, *91*, 251−261. (h) Tan, C.; Chen, C. Emerging Palladiumand Nickel Catalysts for Copolymerization of Olefins with Polar Monomers. *Angew. Chem., Int. Ed.* **2019**, *58*, 7192−7200.

(3) For representative reports since 2014, see: (a) Ota, Y.; Ito, S.; Kuroda, J.; Okumura, Y.; Nozaki, K. Quantification of the Steric Influence of Alkylphosphine−Sulfonate Ligands on Polymerization, Leading to High-Molecular-Weight Copolymers of Ethylene and Polar Monomers. *J. Am. Chem. Soc.* **2014**, *136*, 11898−11901. (b) Jian, Z.; Wucher, P.; Mecking, S. Heterocycle-Substituted Phosphinesulfonato Palladium(II) Complexes for Insertion Copolymerization of Methyl Acrylate. *Organometallics* **2014**, *33*, 2879−2888. (c) Contrella, N. D.; Jordan, R. F. Lewis acid modification and ethylene oligomerization behavior of palladium catalysts that contain a phosphine-sulfonate-diethyl phosphonate ancillary ligand. *Organometallics* **2014**, *33*, 7199−7208. (d) Jian, Z.; Mecking, S. Insertion Homo- and Copolymerization of Diallyl Ether. *Angew. Chem., Int. Ed.* **2015**, *54*, 15845−15849. (e) Chen, M.; Yang, B.; Chen, C. Redox-Controlled Olefin (Co)Polymerization Catalyzed by Ferrocene-Bridged Phosphine-Sulfonate Palladium Complexes. *Angew. Chem., Int. Ed.* **2015**, *54*, 15520−15524. (f) Schuster, N.; Rünzi, T.; Mecking, S. Reactivity of Functionalized Vinyl Monomers in Insertion Copolymerization. *Macromolecules* **2016**, *49*, 1172−1179. (g) Jian, Z.; Leicht, H.; Mecking, S. Direct Synthesis of Imidazolium-Functional Polyethylene by Insertion Copolymerization. *Macromol. Rapid Commun.* **2016**, *37*, 934−938. (h) Wu, Z.; Chen, M.; Chen, C. Ethylene Polymerization and Copolymerization by Palladium and Nickel Catalysts Containing Naphthalene-Bridged Phosphine−Sulfonate Ligands. *Organometallics* **2016**, *35*, 1472−1479. (i) Jian, Z.; Mecking, S. Insertion Polymerization of Divinyl Formal. *Macromolecules* **2016**, *49*, 4395−4403. (j) Jian, Z.; Falivene, L.; Boffa, G.; Sánchez, S. O.; Caporaso, L.; Grassi, A.; Mecking, S. Direct Synthesis of Telechelic Polyethylene by Selective Insertion Polymerization. *Angew. Chem., Int. Ed.* **2016**, *55*, 14378−14383. (k) Wei, J.; Shen, Z.; Filatov, A. S.; Liu, Q.; Jordan, R. F. Self-Assembled Cage Structures and Ethylene Polymerization Behavior of Palladium Alkyl Complexes That Contain Phosphine-Bis(arenesulfonate) Ligands. *Organometallics* **2016**, *35*, 3557−3568. (l) Ota, Y.; Ito, S.; Kobayashi, M.; Kitade, S.; Sakata, K.; Tayano, T.; Nozaki, K. Crystalline Isotactic Polar Polypropylene from the Palladium-Catalyzed Copolymerization of Propylene and Polar Monomers. *Angew. Chem., Int. Ed.* **2016**, *55*, 7505−7509. (m) Wada, S.; Jordan, R. F. Olefin Insertion into a Pd-F Bond: Catalyst Reactivation Following β-F Elimination in Ethylene/Vinyl Fluoride Copolymerization. *Angew. Chem., Int. Ed.* **2017**, *56*, 1820−1824. (n) Chen, M.; Chen, C. Rational Design of High-Performance Phosphine Sulfonate Nickel Catalysts for Ethylene Polymerization and Copolymerization with Polar Monomers. *ACS Catal.* **2017**, *7*, 1308−1312. (o) Yang, B.; Pang, W.; Chen, M. Redox Control in Olefin Polymerization Catalysis by Phosphine−Sulfonate Palladium and Nickel Complexes. *Eur. J. Inorg. Chem.* **2017**, *2017*, 2510−2514. (p) Liang, T.; Chen, C. Side-Arm Control in Phosphine-Sulfonate Palladium- and Nickel-Catalyzed Ethylene Polymerization and Copolymerization. *Organometallics* **2017**, *36*, 2338−2344. (q) Wu, Z.; Hong, C.; Du, H.; Pang, W.; Chen, C. Influence of Ligand Backbone Structure and Connectivity on the Properties of Phosphine-Sulfonate Pd(II)/Ni(II) Catalysts. *Polymers* **2017**, *9*, 168. (r) Black, R. E.; Jordan, R. F. Synthesis and Reactivity of Palladium(II) Alkyl Complexes that Contain Phosphine-cyclopentanesulfonate Ligands. *Organometallics* **2017**, *36*, 3415−3428. (s) Yang, B.; Xiong, S.; Chen, C. Manipulation of polymer branching density in phosphine-sulfonate palladium and nickel catalyzed ethylene polymerization. *Polym. Chem.* **2017**, *8*, 6272−6276. (t) Zhang, D.; Chen, C. Influence of Polyethylene Glycol Unit on Palladium- and Nickel-Catalyzed Ethylene Polymerization and Copolymerization. *Angew. Chem., Int. Ed.* **2017**, *56*, 14672−14676. (u) Song, G.; Pang, W.; Li, W.; Chen, M.; Chen, C. Phosphine-sulfonate-based nickel catalysts: ethylene polymerization and copolymerization with polar-functionalized norbornenes. *Polym. Chem.* **2017**, *8*, 7400−7405. (v) Black, R. E.; Jordan, R. F. Synthesis and Reactivity of Palladium(II) Alkyl Complexes That Contain Phosphine-Cyclopentanesulfonate Ligands. *Organometallics* **2017**, *36*, 3415−3428. (w) Zou, C.; Pang, W.; Chen, C. Influence of Chelate Ring Size on the Properties of Phosphine-Sulfonate Palladium Catalysts. *Sci. China Chem.* **2018**, *61*, 1175−1178.

(4) Wucher, P.; Goldbach, V.; Mecking, S. Electronic Influences in Phosphinesulfonato Palladium(II) Polymerization Catalysts. *Organometallics* **2013**, *32*, 4516−4522.

(5) (a) Verloop, A. In *Drug Design*; Ariens, E. J., Ed.; Academic Press: New York, 1976; Vol. 3, p 133. (b) Verloop, A. In *QSAR in Drug Design and Toxicology*; Hadzi, B. J.-B., Ed.; Elsevier: Amsterdam, 1987; p 97. (c) Harper, K. C.; Bess, E. N.; Sigman, M. S. Multidimensional steric parameters in the analysis of asymmetric catalytic reactions. *Nat. Chem.* **2012**, *4*, 366−374. (d) Ehm, C.; vittoria, A.; Goryunov, G. P.; Izmer, V. V.; Kononovich, D. S.; Samsonov, O. V.; Di Girolamo, R.; Budzelaar, P. H. M.; Voskoboynikov, A. Z.; Busico, V.; Uborsky, D. V.; Cipullo, R. An Integrated High Throughput Experimentation/Predictive QSAR Modeling Approach to ansa-Zirconocene Catalysts for Isotactic Polypropylene. *Polymers* **2020**, *12*, 1005.

(6) The relationship between log(MW) and $\Delta\Delta G$ can be written as

$$\Delta G(\text{TS for chain transfer}) - \Delta G(\text{TS for ethylene insertion}) = RT\ln(\text{DP}) = \frac{RT}{\log e}\log(\text{MW}) - RT\ln(28)$$

where DP is the degree of polymerization, (MW of polymer)/(MW of monomer). This means $\Delta\Delta G$ [kcal/mol] = 1.6 log(MW) − 2.3 at 80 °C.

(7) Hostaš, J.; Řezáč, J. Accurate DFT-D3 Calculations in a Small Basis Set. *J. Chem. Theory Comput.* **2017**, *13*, 3575−3585.

(8) (a) Zahrt, A. F.; Henle, J. J.; Rose, B. T.; Wang, Y.; Darrow, W. T.; Denmark, S. E. Prediction of Higher-Selectivity Catalysts by Computer-Driven Workflow and Machine Learning. *Science* **2019**, *363* (6424), eaau5631. (b) Reid, J. P.; Sigman, M. S. Holistic Prediction of Enantioselectivity in Asymmetric Catalysis. *Nature* **2019**, *571*, 343−348.

(9) Nakano, R.; Chung, L. W.; Watanabe, Y.; Okuno, Y.; Okumura, Y.; Ito, S.; Morokuma, K.; Nozaki, K. Elucidating the Key Role of Phosphine−Sulfonate Ligands in Palladium-Catalyzed Ethylene Polymerization: Effect of Ligand Structure on the Molecular Weight and Linearity of Polyethylene. *ACS Catal.* **2016**, *6*, 6101−6113.

(10) Santiago, C. B.; Guo, J.-Y.; Sigman, M. S. Predictive and mechanistic multivariate linear regression models for reaction development. *Chem. Sci.* **2018**, *9*, 2398−2412.

(11) Martin, Y. C. *Quantitative Drug Design*; Marcel Dekker: New York, 1978.

(12) Clavier, H.; Nolan, S. P. Percent buried volume for phosphine and *N*-heterocyclic carbeneligands: steric properties in organometallic chemistry. *Chem. Commun.* **2010**, *46*, 841−861.

(13) The HOMO and LUMO orbital images are shown in the Supporting Information.

https://doi.org/10.1021/acs.organomet.2c00066
Organometallics 2022, 41, 3185−3196

(14) A case of incorporation ratio of ≪1 was reported: Nakano, R.; Nozaki, K. Copolymerization of Propylene and Polar Monomers Using Pd/IzQO Catalysts. *J. Am. Chem. Soc.* **2015**, *137*, 10934−10937.

https://doi.org/10.1021/acs.organomet.2c00066
Organometallics 2022, 41, 3185−3196